



HAL
open science

Climate change influences chlorophylls and bacteriochlorophylls metabolism in hypersaline microbial mat

Camille Mazière, M. Bodo, M.A. Perdrau, Cristiana Cravo-Laureau, Robert Duran, Christine Dupuy, Cédric Hubas

► To cite this version:

Camille Mazière, M. Bodo, M.A. Perdrau, Cristiana Cravo-Laureau, Robert Duran, et al.. Climate change influences chlorophylls and bacteriochlorophylls metabolism in hypersaline microbial mat. *Science of the Total Environment*, 2022, 802, pp.149787. <10.1016/j.scitotenv.2021.149787>. <hal-03328597>

HAL Id: hal-03328597

<https://hal.science/hal-03328597v1>

Submitted on 28 Jun 2023

HAL is a multi-disciplinary open access archive for the deposit and dissemination of scientific research documents, whether they are published or not. The documents may come from teaching and research institutions in France or abroad, or from public or private research centers.

L'archive ouverte pluridisciplinaire **HAL**, est destinée au dépôt et à la diffusion de documents scientifiques de niveau recherche, publiés ou non, émanant des établissements d'enseignement et de recherche français ou étrangers, des laboratoires publics ou privés.



HAL Authorization

Climate change influences chlorophylls and bacteriochlorophylls metabolism in hypersaline microbial mat

C. Mazière^{1,2*}, M. Bodo³, M. A. Perdrau², C. Cravo-Laureau¹, R. Duran¹, C. Dupuy², C. Hubas³

¹ Université de Pau et des Pays de l'Adour, E2S UPPA, CNRS, IPREM UMR 525 - Bât. IBEAS, BP1155, 64013 PAU cedex, France

² La Rochelle Université, CNRS, UMR 7266 LIENSs (Littoral Environnement et Sociétés)- 2, rue Olympe de Gouges, Bât. ILE, 17000 LA ROCHELLE, France

³ Muséum National d'Histoire Naturelle, UMR BOREA 8067, MNHN-IRD-CNRS-SU-UCN-UA - Station Marine de Concarneau, 29900 CONCARNEAU, France

* Corresponding author: camille.maziere@univ-pau.fr, +33 5 59 40 74 68, Bâtiment IBEAS – avenue de l'Université – 64013 Pau, France ; +33 5 46 50 76 31, Bâtiment Ile – 2, rue Olympe de Gouges – 17000 La Rochelle, France

Keywords: hypersaline microbial mats, ocean acidification, mesocosms, chlorophyll derivatives, phototrophic communities

Abstract

This study aimed to determine the effect of the climatic change on the phototrophic communities of hypersaline microbial mats. Ocean acidification and warming were simulated alone and together on microbial mats placed into mesocosms. As expected, the temperature in the warming treatments increased by 4°C from the initial temperature. Surprisingly, no significance difference was observed between the water pH of the different treatments despite of a decrease of 0.4 unit pH in the water reserves of acidification treatments. The salinity increased on the warming treatments and the dissolved oxygen concentration increased and was higher on the acidification treatments. A total of 37 pigments were

32 identified belonging to chlorophylls, carotenes and xanthophylls families. The higher
33 abundance of unknown chlorophyll molecules called chlorophyll derivatives was observed in
34 the acidification alone treatment with a decrease in chlorophyll *a* abundance. This change in
35 pigmentary composition was accompanied by a higher production of bound extracellular
36 carbohydrates but didn't affect the photosynthetic efficiency of the microbial mats. A careful
37 analysis of the absorption properties of these molecules indicated that these chlorophyll
38 derivatives were likely bacteriochlorophyll *c* contained in the chlorosomes of green
39 anoxygenic phototroph bacteria. Two hypotheses can be drawn from these results: 1/ the
40 phototrophic communities of the microbial mats were modified under acidification treatment
41 leading to a higher relative abundance of green anoxygenic bacteria, or 2/ the highest
42 availability of CO₂ in the environment has led to a shift in the metabolism of green
43 anoxygenic bacteria being more competitive than other phototrophs.

44

45

46 **1. Introduction**

47

48 Since the industrial revolution, the atmospheric greenhouse gases concentration has
49 increased sharply leading to a decrease in the pH of the surface ocean of about 0.1 pH unit
50 (IPCC, 2014). In the coming decades, the ocean acidification will continue, associated with
51 an ocean water warming caused by increasing levels of CO₂ in the atmosphere (Hutchins
52 and Fu, 2017; IPCC, 2014). These climatic perturbations will alter the carbon and nutrients
53 cycles on a global scale (Hutchins and Fu, 2017) and are expected to have a direct impact
54 on all physical, chemical and biological parameters that govern marine organisms life
55 (Hutchins and Fu, 2017). Organisms will be faced with unprecedented changes in future
56 ocean conditions, particularly marine life will be severely affected. On France's Atlantic
57 coasts, the Intergovernmental Panel on Climate Change (IPCC) predicts an increase in
58 surface water temperature of 3 to 4 °C and ocean acidification of 0.4 to 0.45 pH units in its
59 most pessimistic scenario (RCP 8.5) by the end of the century (IPCC, 2014).

60 Research on microorganisms facing climatic changes is scarce compared to that on animals
61 and plants (Cavicchioli et al., 2019; Dutta and Dutta, 2016; Reinold et al., 2019). Microbial
62 mats play important key-roles in marine ecosystems, such as participating in the dynamics of
63 carbon, nitrogen et oxygen cycles. They develop at the water-sediment interface in a large
64 variety of environments including coastal beaches (Bolhuis and Stal, 2011), salterns
65 (Fourçans et al., 2004), hot springs (Dobretsov et al., 2011) and many other coastal/marine
66 environments. These are complex microbial structures containing a great diversity of
67 microorganisms coexisting at microscale according to a vertical stratification due to light and
68 microgradients of oxygen, pH and sulphurs (Fourçans et al., 2008; Jorgensen et al., 1983;
69 Revsbech et al., 1983; van Gemerden, 1993). Despite the stratification, microbial mats are
70 dynamic structures where the migration of microorganisms has been described according to
71 the diel cycle (Fourçans et al., 2008, 2006). Numerous interactions occurs in microbial mats
72 representing thus an ecosystem on its own (Reinold et al., 2019). Microbial mats have a
73 remarkable specific, metabolic and molecular diversity, making them highly adaptable to the
74 changing physico-chemical conditions of the environment (Fourçans et al., 2006) as well as
75 to contamination (Bordenave et al., 2008, 2004a, 2004b).

76 microorganisms are fundamental organisms in the functioning of microbial mats because
77 they are primary producers.

78 Autotrophic microorganisms are fundamental organisms in the functioning of microbial mats
79 because they are the major primary producers. They can be chemotroph such as some
80 Bacteroidetes but the major primary producers in photosynthetic microbial mats are the
81 phototrophic microorganisms (Sørensen et al., 2005). Among them, Cyanobacteria produce
82 organic carbon which is then decomposed in the successive lower layers by different
83 heterotrophs. They also secrete adhesive and protective extracellular polymeric substances
84 (EPS), that form a matrix around the cells (Decho, 1990; Fourçans et al., 2006; Hubas, 2018;
85 Wieland et al., 2003). This matrix is generally composed of sugars, proteins, extracellular
86 DNA and other molecules in smaller proportions (Fourçans et al., 2006; Hubas, 2018;

87 Wieland et al., 2003). However, the composition varies depending on the physiological state
88 of the organisms, the specific diversity, the growth stage of the mat and the physico-chemical
89 conditions of the environment (Decho and Moriarty, 1990; Hubas, 2018; Reinold et al., 2019;
90 Underwood et al., 2004). By binding to sedimentary particles, this matrix stabilises the
91 microbial mat and prevents erosion phenomena (Decho, 1990), but it has many other
92 essential roles such as nutrients supply by the sequestration and accumulation of dissolved
93 and particulate nutrients coming from the water column that can be used by microorganisms,
94 or it also helps microbial communication, or bring a protection against UV radiations (Decho,
95 2000; Flemming and Wingender, 2010; Hubas, 2018). EPS are therefore a major component
96 of microbial mats and remain indispensable for their functioning.

97 Several studies have addressed the impact of climate change on photosynthetic marine
98 microbial communities. Some authors have shown that temperature affects the composition,
99 the photosynthetic performance as well as the growth, biomass and physiology of
100 microphytobenthos (Cartaxana et al., 2015; Hancke and Glud, 2004). Acidification effects are
101 thought to occur mainly at the metabolic level, favouring the growth of some microorganisms
102 (Baragi and Anil, 2016; Black et al., 2019; Hicks et al., 2011) but also photorespiration in
103 diatoms and increasing the number of proton pumps for maintaining intracellular pH
104 homeostasis and respiratory processes (Beardall et al., 2009; Black et al., 2019; Gao et al.,
105 2012). Acidification and warming also affect the characteristics of EPS of diatoms and
106 cyanobacteria with a modification of their composition (Li et al., 2016; Ma et al., 2019).

107 Many studies have highlighted the impact of acidification and warming water separately but it
108 is necessary to consider them together as they can act synergistically (Baragi et al., 2015;
109 Baragi and Anil, 2016; Li et al., 2016). The aim of this study was to simulate an acidification
110 and a water warming on microbial mats on mesocosms according to the RCP8.5 scenario of
111 the IPCC for 2100. Here, the phototrophic microbial communities are described and their
112 potential composition variation will be monitored.

114 2. Material and methods

115

116 2.1 Description of the sampled sites

117

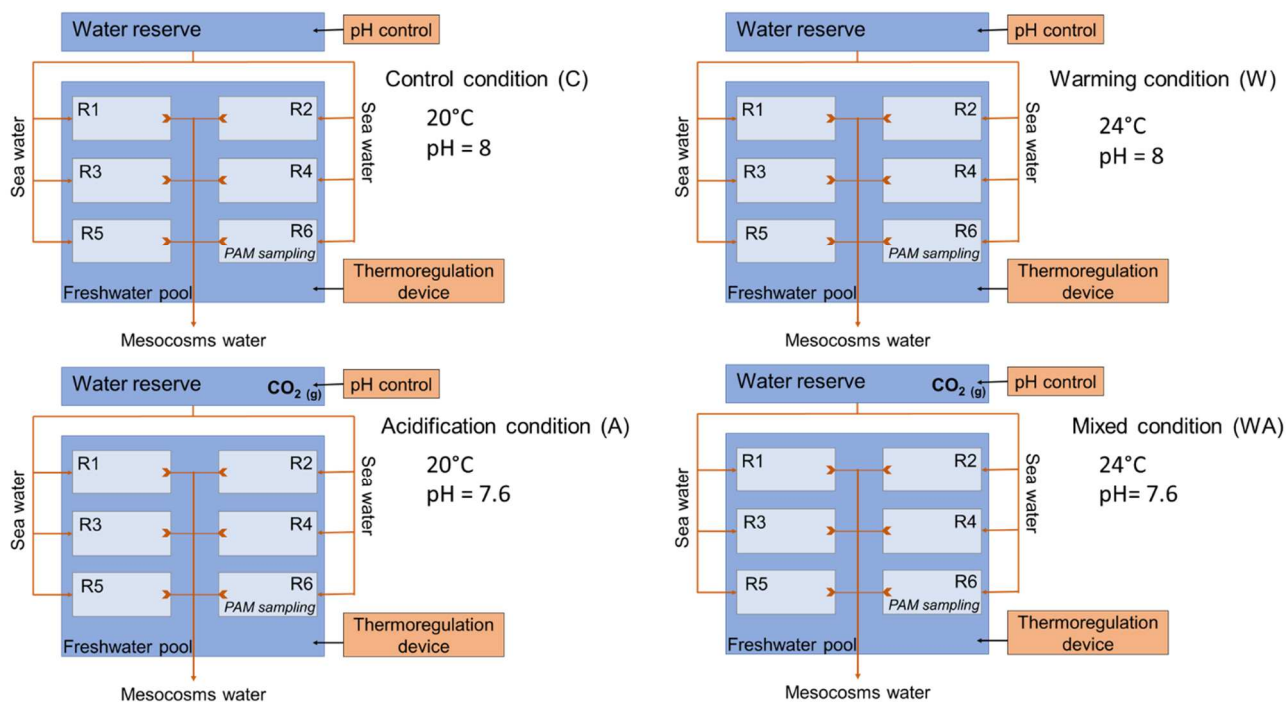
118 Microbial mats for mesocosms experiment were sampled the 30th April 2019 in salterns
119 located in Ars-en-Ré (46°13'29.9"N 1°31'07.5"W, Ré island, France) on a non-exploited
120 pond. The microbial mat, which had not been disturbed for at least three years, was more
121 mature than a mat from an exploited pond. Undisturbed mats were then placed in plastic
122 boxes and transported to laboratory at room temperature where they were put back in water
123 within three hours following the sampling. The water height was around 3 cm as observed *in*
124 *situ*. *In situ* physico-chemical parameters (temperature, salinity, pH) of the water were
125 measured with a multi-parameter probe (pHenomenal® MU 6100H, VWRTM, USA) in order to
126 apply them on the mesocosms as control values. Samples were also taken to determine
127 nutrient salt concentrations in the pore water.

128 2.2 Mesocosm design

129 Microbial mats were separated into twenty-four plastic boxes (48 cm x 33 cm), each of them
130 representing a mesocosm (Fig. 1). The mesocosms were gathered in groups of six
131 representing a condition (five replicates and a box for pulse amplitude modulated (PAM)
132 measures). In these six mesocosms, incoming water was from a reserve and was distributed
133 individually with stainless steel taps. This water corresponded to seawater filtered at 80 µm,
134 passed under UV light and whose salinity was adjusted to 60 psu with salt coming the salt
135 marshes of the Ré island. Opposite to the water inlet, a hole allowed the water outlet in a
136 network of PVC tubes between all the replicates. The water was not recycled. This setup
137 permitted to maintain a stable water level at 3 cm above the mat and to renew seawater and
138 the supplying nutrients for the development of the microbial mats. For each condition, a pool
139 was constructed around the six plastic boxes where water was maintained at the desired
140 temperature with a pump (EHEIM universal 600, Germany) connected to a thermoregulating

141 device (Teco®) to control the water temperature above the microbial mats. The microbial
 142 mats were illuminated twelve hours a day following the day/night cycle observed during the
 143 spring. To control the evaporation rate, the lights used were LED (TOP-24H company by
 144 SYLED, France). They provided white cold light color and an intensity of 11.8 ± 0.9
 145 $\mu\text{mol.photons.m}^{-2}.\text{s}^{-1}$ (mean \pm standard between the four treatments for a day) (HOBO
 146 Pendant® Temperature/Light Data Logger, Onset Computer Corporation, USA) on the
 147 surface of the microbial mats.

148 Daily monitoring was done for the physico-chemical parameters (temperature, pH, salinity
 149 and dissolved oxygen) thanks to a multiparameter probe (pHenomena® MU 6100H, VWR™,
 150 USA).



151

152 **Figure 1:** Schematic representation of the experimental device with the control (C) and the
 153 acidification (A), warming (W) and mixed (WA) treatments. The replicates are represented by
 154 the letter R, the first five are used for sampling and the sixth is dedicated to the
 155 measurements of fluorimetry by pulse amplitude modulation (PAM).

156

157 2.3 Implementation of different treatments

158 A stabilisation period of five weeks was applied to acclimate the microbial mats to their new
 159 environment (Gette-Bouvarot et al., 2015; Stauffert et al., 2013). The water temperature on

160 the mesocosms was maintained at 20°C and the salinity of the incoming water was regulated
161 in the water reserve to maintain a salinity at 60 +/- 2 psu in the mesocosms, reproducing *in*
162 *situ* conditions. The implementation of different treatments occurred for seven additional
163 weeks.

164 Four treatments were applied to the microbial mats. Each pool and its six mesocosms
165 represented a condition. The first treatment was the control treatment (C) in which the
166 parameters were not changed. The second treatment was the warming treatment (W) in
167 which the temperature was increased by 0.5°C every two days for 2 weeks until reaching
168 24°C. The acidification treatment (A) represented the third condition. The water acidification
169 was performed in the water reserve by bubbling pure CO₂, allowing a drop of initial water pH
170 of 0.1 unit every four days for 2 weeks until reaching a decrease of the initial pH of the water
171 reserve equal to 0.4 unit, *i.e.* 7.6. The water pH in the water reserve was monitored with a
172 continuous pH stat system (IKS aquastar, iks ComputerSysteme GmbH, Germany). Then the
173 pH values of the pH stat system were adjusted twice a week from measurement using a pH
174 meter (Metrohm, 826 pH mobile) with a glass electrode (Metrohm, electrode plus) calibrated
175 on the total scale using Tris buffer solution (provided by Andrew Dickson, Scripps Institution
176 Oceanography, San Diego). Every day, the pH values in the four treatments pools were also
177 measured on the total scale. The fourth treatment combined warming and acidification
178 treatments (WA). The mesocosms were then maintained under these treatments for 5 further
179 weeks.

180 A first sampling (noted t₉) was performed after the stabilisation period of the microbial mats
181 on the mesocosms, just before changing the environmental conditions. A second sampling
182 (t₁₆) was performed at the middle of the period of change and a third (t₂₃) at the end
183 (Supplementary materials, fig. A). After this period, sampling was performed every week (t₃₀,
184 t₃₇, t₄₄, t₅₁ and t₅₈) (Supplementary materials, fig. A). For each sampling, ten 1 cm depth
185 cores were collected with a 1 cm diameter cut-off syringe in each mesocosm and mixed
186 together in order to obtain a homogeneous sample.

187 **2.4 Nutrient concentrations**

188 A volume of 20 mL of water from each mesocosm was filtered at 0.22 μm in order to perform
189 a nutrient analysis. The same was done for *in situ* samples. Half of the volume was frozen at
190 -20°C while the other half was kept at 4°C for silicon analysis. The samples were then
191 analyzed as described by Aminot and K  rouel (2007). Silicon, nitrate, nitrite and phosphate
192 were measured by Segmented Continuous Flow Colorimetry (SFA) while ammonium was
193 measured by SFA fluorimetry on an auto-analyser (SEAL AutoAnalyzer 3, SEAL analytical)
194 (Aminot and K  rouel, 2007).

195 **2.5 Photosynthetic parameters**

196
197 Chlorophyll fluorescence parameters were measured at 5 different locations of the core using
198 a fluorometer (Monitoring Pen, MP 100-E, Photon Systems Instruments, Czech Republic)
199 illuminated with a blue LED emitter (455 nm). The samples were placed in the dark (for 5
200 min) before the measurement of Light Response Curves. Manufacturer predetermined LC3
201 protocol was used following manufacturer instructions. LC3 protocol was characterised by 7
202 steps of increasing light intensities (10, 20, 50, 100, 300, 500, 1000 $\mu\text{mol.photon.m}^{-2}.\text{s}^{-1}$) with
203 an illumination duration of 60s. Minimum fluorescence level F_0^5 (Jesus et al., 2006) was
204 obtained by using a non actinic measuring light pulse (30 μs , 900 $\mu\text{mol.photon.m}^{-2}.\text{s}^{-1}$), which
205 induced the minimal chlorophyll fluorescence (F_0^5). The samples were then subjected to a
206 saturating light pulse (2,400 $\mu\text{mol.photon.m}^{-2}.\text{s}^{-1}$). This made it possible to measure the
207 maximum fluorescence level F_m^5 (Jesus et al., 2006). All measurement were done in the
208 same conditions and at the same time.

209 The data was then downloaded from the device to a computer using FluorPen software
210 (v1.0.6.1, Photon Systems Instruments, Czech Republic) and all calculations and analyses
211 were performed using R.Studio software (version 4.0.3^{  } RStudio, Inc.). From the measured
212 parameters the effective quantum yields of photosynthesis ($\phi(II)^5$) were calculated (Jesus et

213 al., 2006) (Equation 1). They indicate the community's maximum potential for photosynthetic
214 activity.

$$\phi(II)^5 = \frac{F_m^5 - F_0^5}{F_m^5} \quad (\text{Equation 1})$$

215

216

217 **2.6 Pigment identification and quantification**

218

219 Lipophilic pigments were analyzed by high performance liquid chromatography (HPLC).
220 Microbial mats were incubated with 95% methanol (buffered with 2% ammonium acetate)
221 during 15 min, at -20°C in the dark. Extracts were then filtered with 0.2µm PTFE syringe
222 filters and analyzed within 16h using an Agilent 1260 Infinity HPLC composed of a
223 quaternary pump (VL 400 bar), a UV–VIS photodiode array detector (DAD 1260 VL, 190–950
224 nm), a fluorescence detector (FLD 1260 excitation: 425 nm, emission: 655 nm), and a 100µl
225 automatic sample injector refrigerated at 4°C in the dark. Chromatographic separation was
226 carried out using a C18 column for reverse phase chromatography (Supelcosil, 25 cm long,
227 4.6 mm inner diameter). The solvents used were: 0.5M ammonium acetate in methanol and
228 water (85:15, v:v), acetonitrile and water (90:10, v:v), and 100% ethyl acetate. The solvent
229 gradient was set according to Brotas and Plante-Cuny (2003), with a 0.5 mL min⁻¹ flow rate.
230 Identification and calibration of the HPLC peaks were performed with $\beta\beta$ -carotene,
231 canthaxanthin, chlorophyll *a*, chlorophyll *b*, chlorophyll *c2*, diatoxanthin, diadinoxanthin,
232 fucoxanthin and pheophytin *a* standards. We identified all detected peaks by their absorption
233 spectra and relative retention times using the Agilent OpenLab software. Quantification was
234 performed using standard calibration curves built with repeated injections of standards over a
235 range of dilutions. Xanthophylls, carotens and chlorophyll *b* and *c* were quantified at 470 nm,
236 chlorophyll *a* and their derivatives as well as pheopigments were quantified at 665 nm. The
237 relative abundance of each pigment (%) was calculated from its respective concentration in
238 the sample (µg.mg⁻¹).

239

2.7 Extracellular Polymeric Substances (EPS) characterization

240 In a 15 mL Falcon® tube, 5 mL of microbial mat was mixed with an equivalent volume of
241 seawater obtained by mixing water from the five sampled replicate and filtered at 0.22 µm for
242 each treatment. The tubes were subjected to mechanical agitation by vortexing and by
243 inversion at a rate of 40 oscillations.min⁻¹ for 1 h at 4°C in the dark. Then they were
244 centrifuged at 3500 g for 10 min at 4°C. The supernatant, containing the colloidal fraction,
245 was recovered and stored at -20°C while the pellet, containing the bound fraction, was
246 resuspended in 5 mL of seawater (again obtained by mixing water from the five sampled
247 replicate and filtered at 0.22 µm for each treatment). 1 g of Dowex resin (Dowex Marathon C,
248 Na⁺, Sigma-Aldrich), was prepared according to the protocol of Takahashi *et al.* (2009). The
249 tubes were again subjected to the same protocol to obtain the supernatant containing the
250 fraction of bound EPS was recovered and stored at -20°C.

251 The carbohydrate dosage was performed according to Dubois' colorimetric method (Dubois et
252 al., 1956) while the protein dosage was performed according to the BiCinchoninic acid Assay
253 (BCA) method using the Pierce™ Protein Assay Kit (Thermoscientific). A range of glucose (L-
254 (-)-Glucose, 98%, Sigma-Aldrich) from 0 to 3 g.L⁻¹ and a range of bovine serum albumin
255 (BSA) from 0 to 1 g.L⁻¹ were performed in seawater from the Ré island hypersalinated at 60
256 psu and filtered at 0.22 µm. For carbohydrates, 100 µL of EPS sample were placed in a tube,
257 then 100 µL of 5% phenol (Solid Phenol, Sigma-Aldrich, France) and 500 µL of 98%
258 sulphuric acid (Sulphuric Acid 98%, Carlo-Erba Reagents, France) were added. The tubes
259 were incubated for 30 min in the dark and at room temperature. A volume of 200 µL of the
260 standard range and each triplicate sample was deposited in a 96-well microplate (Falcon® 96-
261 well Clear Microplat, Thermo Fisher Scientific). The absorbance of each well was measured
262 at 490 nm with a spectrophotometer (SPECTROstar® Nano, BMG LAB). For proteins, 225 mL
263 of reagent was prepared and stored in the dark at room temperature during the assay period.
264 The assays were performed in 96-well microplates (Falcon® 96-well Clear Microplat, Thermo
265 Fisher Scientific). 200 µL of reagents were placed in the wells and 25 µL standards or

266 triplicate samples were added. The microplates were incubated for 30 min at 37°C, then the
267 absorbance of each sample was measured at 562 nm by a spectrophotometer
268 (SPECTROstar® Nano, BMG LAB). Two calibration curves were drawn from the standard
269 ranges and their respective abundances (corrected according to the kit indications for the
270 BSA range), averaged over the duration of the experiment. They made it possible to
271 determine the carbohydrate and protein concentrations. The latter were then related to the
272 dry mass of the microbial mat.

273 To determine the dry mass of the microbial mat, a volume of 30 mL of microbial mat was
274 collected and weighed to obtain the fresh mass (M_F). The sample was then freeze-dried to
275 remove water from the sample (Lyophilisateur Christ Alpha 1-4, Grosseron, France) and re-
276 weighed to obtain the freeze-dried mass (M_L).

277 **2.8 Data analysis**

278 All calculations and analyses were performed on R.Studio software (version 4.0.3® RStudio,
279 Inc.). The mean of physico-chemical parameters, the carbohydrates and proteins
280 concentrations of each fraction and the photosynthetic parameters of each treatment were
281 compared with each other at each sampling time. The normality and homoscedasticity of the
282 data were previously verified by carrying out a Shapiro test and a Bartlett test respectively. If
283 both conditions were met, the data were subjected to an analysis of variances (ANOVA).
284 Otherwise, a Welch ANOVA was performed in the case of non-homogeneity of variances and
285 a Kruskal-Wallis rank sum test in the case of non-normal data. If these tests were found to be
286 significant ($p < 0.05$), then a pairwise comparison was performed using a Tukey test following
287 the ANOVA, a Games-Howell test following a Welch ANOVA or a Nemenyi test following the
288 Kruskal-Wallis test.

289 A Between Class Analysis (BCA) combined with hierarchical cluster analysis with a Bray
290 dissimilarity index and ward.D2 method was done on pigments proportions.

291 **3. Results**

292

293 **3.1 Efficiency of the physico-chemical changes**

294

295 As expected, the temperature in W and WA treatments increased well by 4°C from the initial
296 temperature, the one maintained in C and A treatments ($23.89 \pm 0.49^\circ\text{C}$; $23.82 \pm 0.48^\circ\text{C}$;
297 $20.32 \pm 0.36^\circ\text{C}$; $20.23 \pm 0.48^\circ\text{C}$; respectively) (Fig. 2, A; Supplementary materials, fig. B).
298 There was a delay of one week before reaching this increase after the change of state
299 because this was the time needed to heat up all the water in the pool and then the
300 mesocosms.

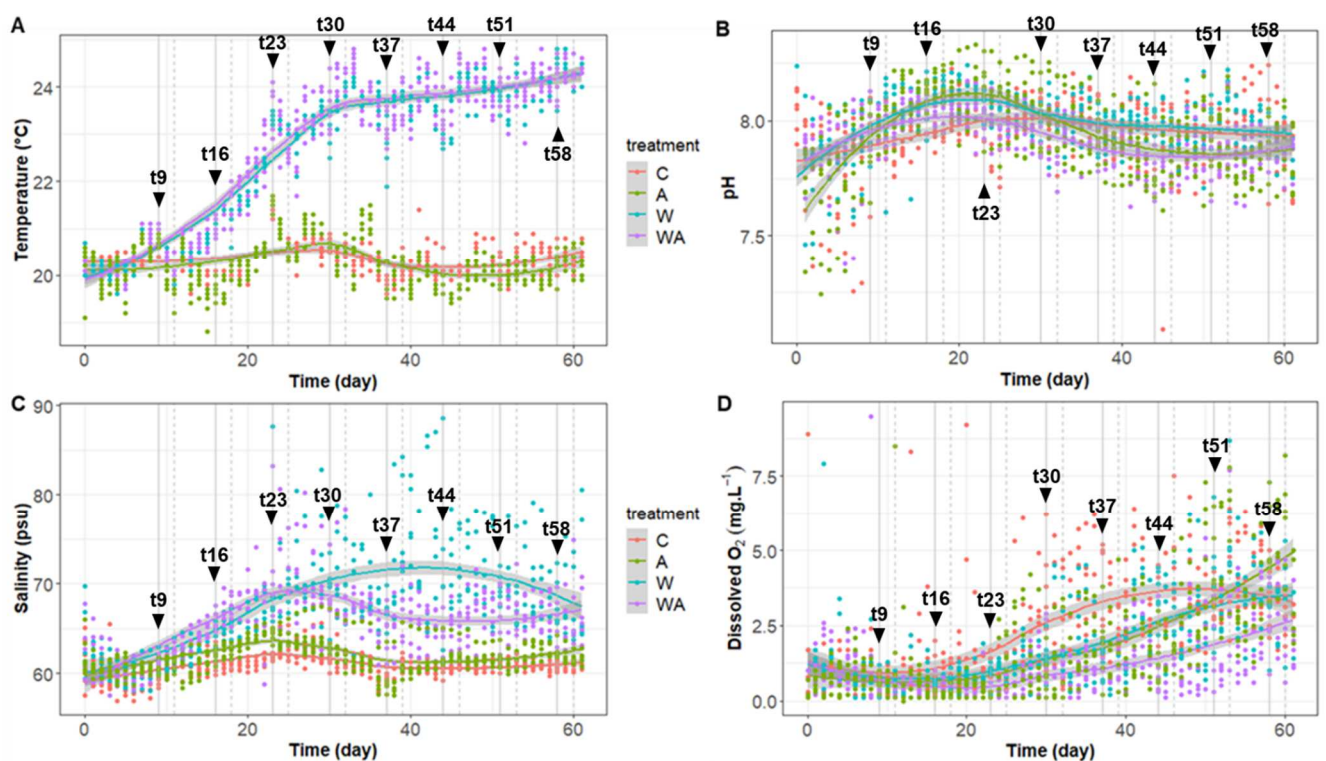
301 The pH of C and W treatments were stabilized after t37 at 7.94 ± 0.15 and 7.95 ± 0.09 ,
302 respectively (Fig.2, B; Supplementary materials, fig. B). The pH of A and WA treatments
303 decreased until t44, then remaining stable at pH 7.87 ± 0.13 and 7.86 ± 0.10 , respectively
304 (Fig.2, B; Supplementary materials, fig. B). No significant difference between the four
305 treatments was found at t9 (Kruskal, $p > 0.05$).

306 The salinity (Fig. 2, C; Supplementary materials, fig. B) of C and A treatments remained
307 stable at 60.87 ± 1.44 psu and 61.91 ± 1.79 psu, respectively. The salinity of the W treatment
308 increased to a maximum mean value of 75.87 ± 4.84 psu after 40 days of incubation, and
309 then decreased again to a final value of 67.35 ± 4.24 psu. The salinity of the WA treatment
310 increased and reached its maximum value of 71.94 ± 6.55 psu on day 23 of the experiment
311 and then decreased and remained at 66.13 ± 2.56 psu.

312 Dissolved oxygen remained stable between each treatment up to t16 (mean \pm standard
313 deviation; 0.95 ± 1.18 mg.L⁻¹ for control, 0.61 ± 1.15 mg.L⁻¹ for pH, 0.60 ± 0.46 mg.L⁻¹ for W
314 and 0.30 ± 0.24 mg.L⁻¹ for WA) (Fig. 2, D; Supplementary materials, fig. B). From t23, the
315 dissolved oxygen of the treatments increased linearly to t58 with a slope of 0.07 day⁻¹ ($R^2 =$
316 0.45 , Student-test, $p < 0.05$) for A, 0.05 day⁻¹ ($R^2 = 0.39$, Student-test, $p < 0.05$) for W and
317 0.03 day⁻¹ ($R^2 = 0.19$, Student-test, $p < 0.05$) for WA. The A treatment had a final oxygen
318 concentration of 5.95 ± 1.63 mg.L⁻¹, significantly higher (ANOVA, $p < 0.05$) than that of the

319 other mesocosms by a factor of 1.6 for W, 2.2 for C and 2.4 for WA (mean \pm standard
320 deviation).

321 The nutrients were analyzed thanks to the Redfield ratio calculations (Redfield, 1958). Only
322 seven samples showed nitrogen limitation, notably four replicates of the A treatment at t30
323 and some samples showed a limitation of silicon (Supplementary materials, fig. B and C).
324 Most of the samples showed phosphate limitation, but such phosphate limitation was also
325 observed *in situ* (Supplementary materials, fig. B and C).



326 **Figure 2:** Temporal variation of the temperature (°C) (A), the pH (upH) (B), the salinity (psu)
327 (C) and the dissolved oxygen (mg.L⁻¹) (D) of the different treatments (control (C), acidification
328 (A), warming (W) or warming and acidification mix (WA)). The points corresponded to the
329 values measured for each sample. The curves represented local regressions, based on the
330 k-nearest neighbors algorithm (*geom_smooth* function of the *ggplot2* package, loess
331 method). The grey areas symbolised the 95% confidence intervals. The sampling days were
332 represented by black arrows. The day 0 to day 8 corresponded to the stabilisation week.
333

334

335 3.2 Pigment composition

336

337 A total of 37 pigments were identified. The analysis revealed the presence of several
338 chlorophyll: chlorophyll *a* (Ca) and corresponding epimers and allomers, chlorophyll *b* (Cb)

339 and chlorophyll *c2* (Cc2). Bacteriochlorophyll *a* (BCa) was identified as well as echinenone,
 340 oscillol diquinoside, myxol quinovoside and zeaxanthin. Other pigments were identified
 341 including lutein, alloxanthin, carotenoids and canthaxanthins and its isomers. Pigments
 342 corresponding to alteration products were also found: pyropheophytin, pheophytin *a*,
 343 pheophorbide *a* and chlorophyllide *a*. The presence of non-identified chlorophyll *a*-like
 344 molecules was also observed and hereby called chlorophyll derivatives (C deriv. #1-6).

345 **Table 1:** Pigments identified by HPLC and its corresponding abbreviations.

Pigment	Notation
alpha and beta Cryptoxanthin	aCy; bCy
Alloxanthin	Al
Beta-beta caroten; beta-epsilon caroten	BB.Car; BE.Car
Unknown carotenoids	Car1; Car2
Chlorophyll <i>a</i> ; Chlorophyll <i>a</i> allomers/epimers	Ca; Ca.allo; Ca.epi
Chlorophyll derivatives	C deriv. #1-6
Bacteriochlorophyll <i>a</i>	BCa
Chlorophyll <i>b</i>	Cb
Chlorophyll <i>c2</i>	Cc2
Chlorophyllide <i>a</i>	Cda
Canthaxanthin	Ct; Ct.iso
Echinenone	Ec
Fucoxanthin and isomers	F; F.iso1
Lutein and isomers	L; L.iso1; L.iso2
Myxol quinovoside and isomers	My.iso1; My.iso2; My.iso3; My.iso4
Oscillol diquinoside	O
Pheophorbide	Pda.1
Pheophytin	Pha
Pyropheophytin	Pya
Zeaxanthin	Z

346

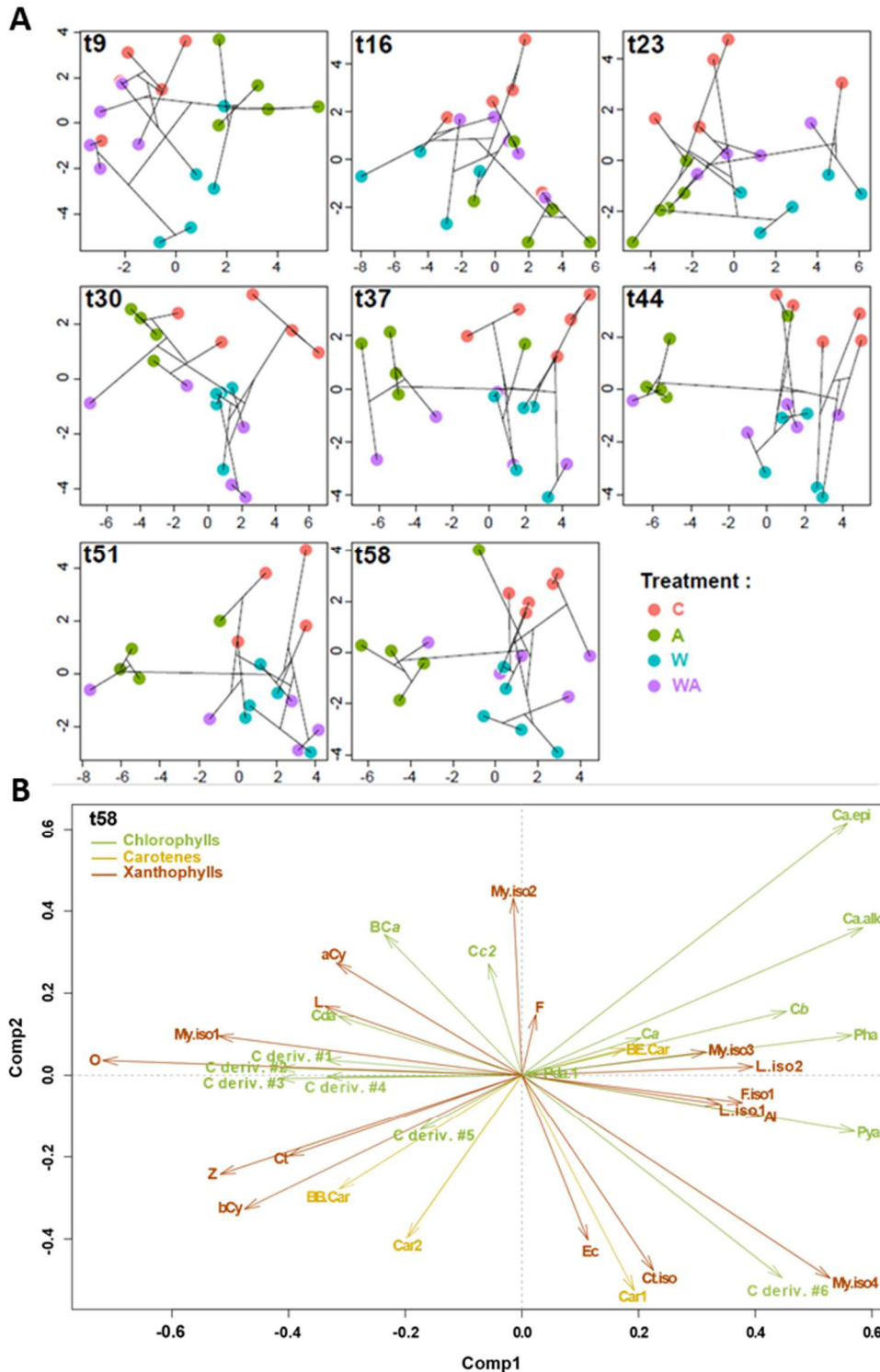
347 **3.3 Acidification changes the pigments dynamics**

348

349 At t9, all treatments were placed under the same water temperature and pH. No difference
 350 between pigments were observed (Fig.3) (ANOVA or Welch or Kruskal, $p>0.05$).

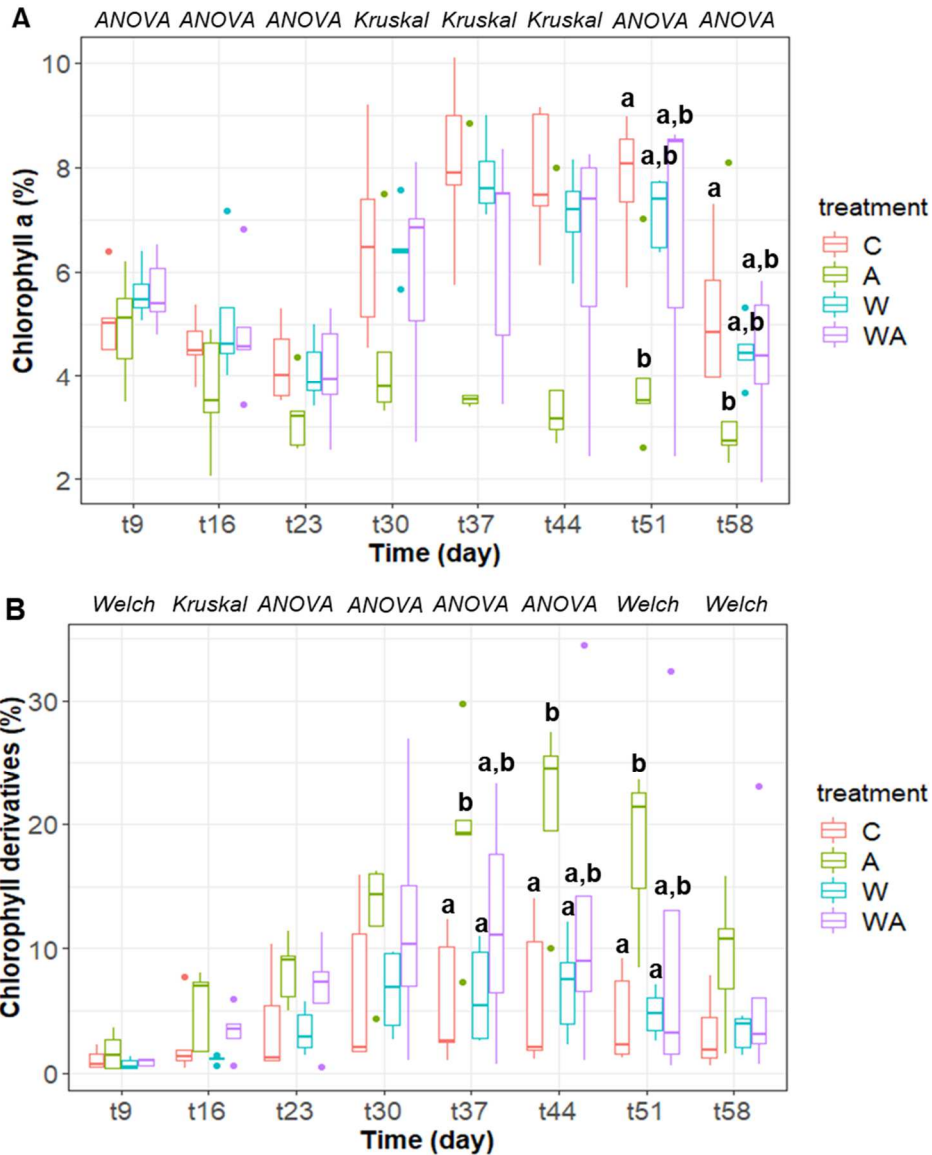
351 The C treatment was different form the other treatments containing more myxol quinovoside
 352 and isomers 2 and 3 than A treatment at t37 and t44 (Kruskal, $p<0.05$) and than the three
 353 other treatments at t51 (ANOVA, $p<0.05$). It also contained more chlorophyll epimers at t58
 354 than A, W and WA treatments (ANOVA, $p<0.05$) (Fig.3). The W treatment was differentiated
 355 from the A treatment with the presence of chlorophyll derivative #6 at t51 and t58 (Welch,

356 $p < 0.05$) (Fig.3). The concentration of chlorophyll *a* was around 4% at the beginning of the
357 experiment (Fig. 4, A). It increased until t51 in all treatments except for A treatment and then
358 decreased at t58 (Fig. 4, A). The A treatment slightly decreased at t58 and the proportion of
359 chlorophyll *a* was lower in this treatment than in the C treatment (ANOVA, $p < 0.05$) at t51
360 and t58 (Fig. 4, A). Conversely, the proportion of chlorophyll derivatives (Fig. 4, B) was close
361 to 0 at t9 for all treatments. It increased to t30, remained stable at t44 and then decreased
362 again to t58 for the C, W and WA groups, while it increased to t44 before decreasing again to
363 t58 for the A group (Fig. 4, B). The proportion of chlorophyll derivatives was significantly
364 higher for the A treatment at t37, t44 and t51 (ANOVA and Welch, $p < 0.05$) (Fig. 4, B).



365

366 **Figure 3:** Dynamics of microbial communities according to pigments composition and the
 367 sampling time (tX) **(A)**. This figure was obtained thanks to analyze BCA combined with
 368 hierarchical cluster analysis with a Bray dissimilarity index and ward.D2 method. A
 369 representation more detailed with the different parameters was done at t58 **(B)**. The
 370 correspondence between the abbreviations and the names of pigments is provided on the
 371 **table 1**.



372

373

374 **Figure 4:** Temporal variations of **(A)** the concentration of chlorophyll a (%) and **(B)** the
 375 concentration of chlorophyll derivatives (%). The letters t followed by a number indicates the
 376 sampling time. The statistical test performed to show the differences between treatments at a
 377 sampling time is indicated in italics above the figure. The letters indicated a significant
 378 difference ($p < 0.05$) found after a post-hoc Tuckey test in the case of an ANOVA or a
 379 Games-Howell test in the case of a Welch ANOVA.

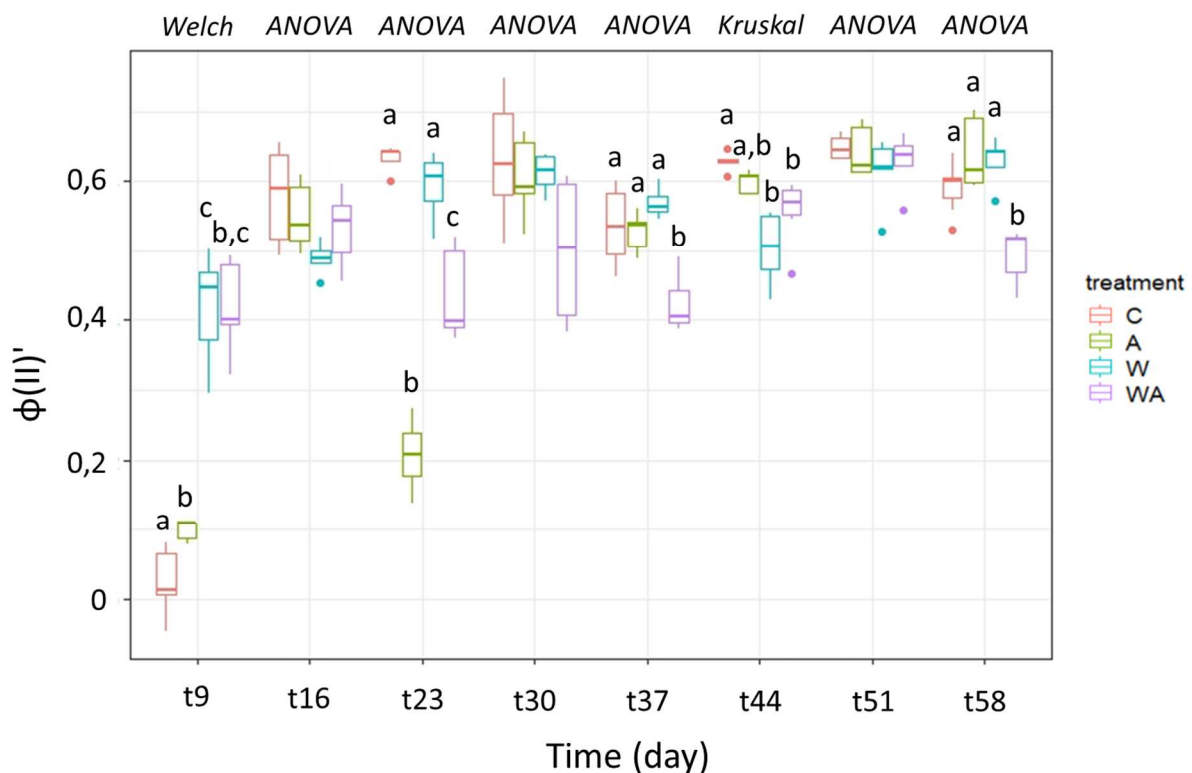
380

381 **3.4 Comparison of the photosynthetic yields of the microbial mat in the** 382 **different treatments**

383

384 The quantum efficiency of photosystem II ($\phi(II)'$) indicated the photosynthetic efficiency of the
 385 mat. At t9, the quantum yields of the C and A treatments were close to 0, while those of the

386 W and WA groups were 14 and 4.2 times more than C and A treatments respectively (Fig. 5).
 387 At t16 no significant difference was observed between all the quantum yields (ANOVA, $p >$
 388 0.05) (Fig. 5). Other difference were observed between treatments during the experiment,
 389 but the kinetics obtained showed no real trend between treatments (Fig. 5), only WA
 390 treatment presented a quantum yields lower than C treatment at t37, t51 and t58 (ANOVA or
 391 Kruskal, $p < 0.05$) than W and A treatments at t37 and t58 (ANOVA, $p < 0.05$).



392

393 **Figure 5:** Variation of the quantum efficiency of photosystem II ($\phi(II)'$) in the different
 394 treatment. The letters t followed by a number indicates the sampling time. Above the figure
 395 was indicated in italics the test carried out for the comparison between treatments of the
 396 same week. The letters indicated a significant difference ($p < 0.05$) found after a post-hoc
 397 Tukey HSD test in the case of an ANOVA, a Games-Howell test in the case of a Welch
 398 ANOVA or a Nemenyi test in the case of a Kruskal Wallis test.

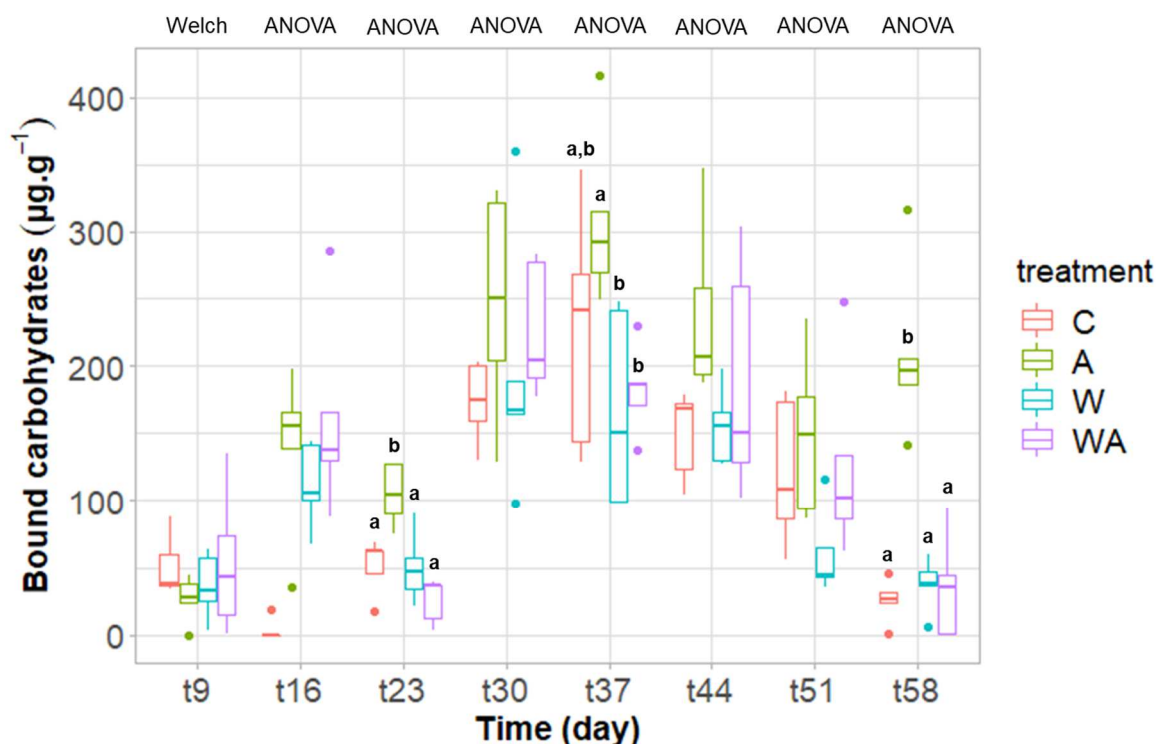
399

400 3.5 Acidification impacted the proportion of EPS

401

402 The A treatment was dissimilar from the other treatments, characterized by its higher
 403 concentrations of bound carbohydrates EPS.

404 The carbohydrates bound EPS concentration was notably more important in A treatment on
 405 three times: at t23, t37 and t58 (ANOVA, $p < 0.05$) (Fig. 6).



406

407 **Figure 6:** Temporal variation of the carbohydrate concentration in the bound fraction of EPS
 408 (in $\mu\text{g.g}^{-1}$ dry mass). The letters t followed by a number indicates the sampling time. The
 409 statistical test performed to show the differences between treatments at a sampling time is
 410 indicated in italics above the figure. The letters indicate a significant difference ($p < 0.05$)
 411 found after a post-hoc Tuckey test. Note: the ANOVA performed at t16 did not consider the C
 412 treatment because of the presence of outliers.

413

414 **4. Discussion**

415

416 The aim of the study was to simulate acidification and/or warming on microbial mats. The
 417 mesocosm system has the advantage to control the physico-chemical parameters allowing to
 418 simulate future conditions, which is impossible to achieve directly in the field; but the natural
 419 environment can never be mimicked perfectly (weather, daily or even seasonal variations in
 420 physico-chemical parameters, *etc.*). Although mesocosm system will never faithfully
 421 represent reality, it is a compromise often used to conduct experimental ecology studies
 422 (Cravo-Laureau and Duran, 2014). It is therefore advisable to remain vigilant so as not to

423 extrapolate too generally the results obtained with *in situ* microbial mats. Given the diversity
424 of structure and functioning of microbial mats throughout the world, they may act differently in
425 their natural environment. It should also be noted that this study was a simulation of the
426 IPCC's most pessimistic predictions (RCP8.5) for 2100. The changes simulated only
427 concerned the decrease in water pH and the increase in water temperature, but these are
428 not the only parameters that are expected to vary in the future. Deoxygenation of the oceans,
429 a succession of extreme weather events, and sea level rise in some regions are also
430 foreseeable changes that have not been tested in this study. Moreover, they have been
431 monitored over seven weeks, whereas variations in the natural environment are supposed to
432 occur over several decades.

433 The renewal water in the mesocosm permitted to maintain a stable water level at 3 cm above
434 the mat and a natural supply of nutrients for the development of microbial mats. Redfield
435 ratio showed some limitation of nitrogen and/or phosphorus in the water under some
436 conditions but previous studies have shown that microbial mats can develop in P- (Peimbert
437 et al., 2012) and N-limited environment (Peimbert et al., 2012) (Supplementary materials, fig.
438 C).

439 Surprisingly, the decrease of pH under the A and WA treatments was not noticeable in the
440 mesocosms (Fig. 2) although the pH in the respective water reserve decreased
441 (Supplementary materials, fig. D) at the expected pH 7.6 (the initial pH was 8). This
442 phenomenon has been observed in other studies (Crawford et al., 2011; Ma et al., 2019).
443 The most likely hypothesis is that the rate of CO₂ fixation by photosynthesis was higher in the
444 A and WA treatments, which had the effect of increasing the pH. In our experiment, dissolved
445 oxygen increased under A treatment after the third week. Moreover, many microbial species
446 are able to use carbon concentration mechanisms (CCMs), storing high CO₂ concentrations
447 before transport into the Rubisco compartments, which minimise photorespiration. These
448 CCMs are found in oxygenic phototrophs like cyanobacteria or most of the phytoplankton
449 (Ma et al., 2019). The CCMs have been proposed as mechanisms to prevent photosynthetic

450 systems to directly detect ambient changes in CO₂ (Mackey et al., 2015). As a result,
451 photosynthetic rates might not respond directly to ambient changes in CO₂ explaining the
452 delay observed in the increase of dissolved oxygen in our experiment. Such observation is
453 consistent with the fact that pH decreased from t23 while dissolved oxygen continued to
454 increase (Fig. 2). Black et al. (2019) suggested that microphytobenthos use additional CO₂
455 due to acidification for photosynthesis until the maximum yield capacity has been reached.
456 When the cells reached maximum intracellular CO₂ concentration through their CCMs, any
457 additional CO₂ would contribute to the decrease in pH. The pH of the WA treatment followed
458 the same dynamic as observed for the A treatment. However, the dissolved oxygen
459 concentration under WA treatment increased less than half in comparison to the A treatment
460 (Fig. 2, D). The CO₂ absorption mechanisms may have been less efficient in WA treatment
461 because temperature decreases the solubility of CO₂ (Wootton et al., 2008).

462 Numerous studies have shown that photosystem II is very sensitive to environmental stress
463 (Murata et al., 2007; Nishiyama et al., 2008; Wang et al., 2013). It is therefore important to
464 focus on the quantum yield of photosystem II, which indicates the maximum photosynthetic
465 activity potential of the communities. At t9, the quantum yield of photosystem II for the C and
466 A treatments were close to 0 (Fig. 5), which indicated that the mats were not in good
467 physiological condition when starting the experiment. Significantly lower quantum yields were
468 observed under some treatments. At t23, under the A and the WA treatments an unexplained
469 decrease of the quantum yield was observed (Fig. 5). The WA treatment exhibited
470 significantly lower quantum yield than the other treatments at t37, t51 and t58 (Fig. 5),
471 suggesting that mats have more difficulty withstanding simultaneous acidification and
472 heating. It was not surprising that there was no difference in quantum efficiency between A
473 and C treatments (Fig. 5). Photosynthetic organisms have a high capacity to modify pH with
474 evidence that pH is regulated at the water/cell interface (Black et al., 2019). Our fluorometer
475 illuminated with a blue LED emitter (455 nm). Chlorophyll *a* fluorescence per unit
476 concentration in cyanobacteria tends to be lower than in algae when it is excited with blue

477 light. This leads to an erroneous biomass estimate of cyanobacteria. In their study, Simis *et*
478 *al.* (2012) have sought the optimal excitation and emission pairs for the separation of
479 cyanobacterial and algal Fv/Fm in communities. They demonstrate that the highest
480 correlation between community and cyanobacterial variable fluorescence is obtained under
481 orange-red excitation in the 590–650 nm range, exciting cyanobacterial phycobilipigments.
482 No information was found about the other phototrophic communities.

483 The A treatment possessed more chlorophyll derivatives and lower chlorophyll *a* than the
484 other treatments (Fig. 4). These chlorophyll derivatives molecules seemed to be bioindicators
485 of a stress condition (water acidification). They were not identified by available standards.
486 These molecules did not correspond to known metallised allomers or epimers of chlorophyll
487 *a* (Ca), as revealed by their retention time (Supplementary materials, fig. E). Based on their
488 absorption spectra (Fig. 7), we can also rule out the hypothesis that these molecules
489 correspond to de-metallised derivatives of chlorophyll *a* such as pheophytin *a* or
490 pheophorbide *a* or even to bacteriochlorophyll *a* (BCa).

491 We can assume that these molecules correspond to transmetalated Ca or BCa. Some
492 microorganisms are known to possess bacteriochlorophyll those the central Mg ion is
493 replaced by another metal, as observed for *Acidiphilium* where BCa possess a Zn central
494 metal (Hiraishi and Shimada, 2001). This organism has been isolated from acidic mine ponds
495 and it is supposed likely that pH constituted the evolutionary pressure responsible for the
496 change of the central metal (Hiraishi and Shimada, 2001). Although this is an attractive
497 hypothesis, it is highly unlikely that our pH treatment had the effect of promoting the
498 synthesis of transmetalated BCa as Zn-BCa displays absorption features in the near infra-red
499 range (Nagata *et al.*, 2003) that were not observed here.

500 Chlorophylls and porphyrin derivatives generally have two major absorption bands (*i.e.* “red”
501 (Q-) and “blue” (Soret-) bands, Fig. 7) in the visible range, due to extended π -delocalization
502 at the edge of cyclic porphyrin skeleton (Milenković *et al.*, 2012). Two main Q-bands ($Q_{y,0-0}$
503 and $Q_{y,0-1}$) are traditionally observed in the original Ca (or Mg-Ca) (Gerola *et al.*, 2011). In our

504 case, Ca wavelengths of maximum absorption λ_{\max} were respectively 665 ($Q_{y,0-0}$) and 615 nm
505 ($Q_{y,0-1}$).

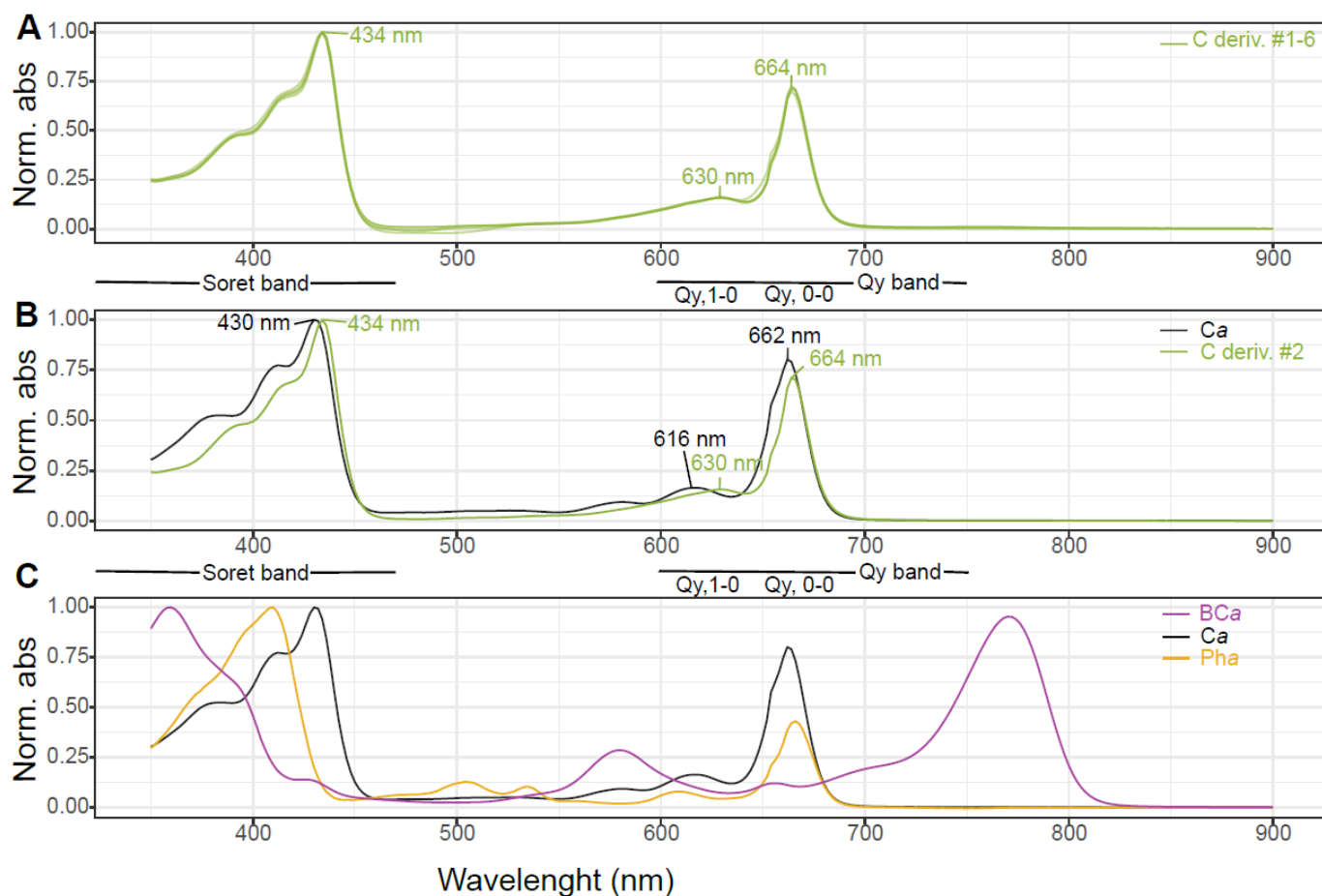
506 Based on these findings, the unidentified derivatives do not correspond to transmetalated
507 Ca, although those absorption characteristics are close to the Mg-Ca molecule. As shown
508 previously by Gerola *et al.* (2011), a hypsochromic (blue) shift of both Soret and $Q_{y,0-0}$ bands
509 must be expected with significant decreasing of λ_{\max} in Zn- and Cu-Ca in comparison to Mg-
510 Ca. Such hypsochromic shifts were not observed in the unidentified derivatives spectra.

511 The only noticeable change corresponded to a decreased intensity (hypochromic effect) in
512 the $Q_{y,0-0}$ band in comparison with that of Mg-Ca and a bathochromic (red) shift in the $Q_{y,0-1}$.
513 (Fig.7). These characteristics are similar to those of bacteriochlorophyll *c* (BC*c*) with a
514 recorded λ_{\max} (630 nm) for $Q_{y,0-1}$ close to the expected 623-629 nm (Goedheer, 1966; Oelze,
515 1985; Pierson and Castenholz, 1974). This pigment is typically found in the chlorosomes of
516 green anoxygenic phototroph bacteria, including the green sulfur bacteria and the green non-
517 sulfur bacteria (Frigaard *et al.*, 2006; Scheer, 2006), which indicated that the pH conditions
518 may have favoured the growth of these phototrophic bacteria.

519 Even moderate changes of both pH and temperature are relevant for bacterial community
520 composition of microbial mats (Uribe-Lorío *et al.*, 2019). A decrease in chlorophyll *a* has
521 been observed under high CO₂ levels suggesting that the CO₂ input reduce CCMs and thus
522 save energy, particularly in pigment synthesis (Wang *et al.*, 2019; Yue *et al.*, 2019). In hot
523 springs from Costa Rica, significant changes of microbial mat communities were observed
524 with a significant increase of Chloroflexi (also named the green non-sulfur bacteria)
525 abundance with decreasing pH and increasing temperature (Uribe-Lorío *et al.*, 2019).
526 Chloroflexi have been previously reported to be more abundant at decreased pH on
527 sediment of hydrothermal CO₂ seeps in Papua New Guinea (Hassenrück *et al.*, 2016) and in
528 host-association with corals and sponges (Kandler *et al.*, 2018; Morrow *et al.*, 2015).
529 Chlorobi, the green sulfur bacteria, have also been found to increase in abundance with
530 acidification (Hassenrück *et al.*, 2016). On their study, Hassenrück *et al.* (2016) supposed

531 that in the sites characterized by low pH and high hydrothermal influence, including
 532 pronounced temperature increases, the Chloroflexi and Chlorobi replaced other microbial
 533 communities as major carbon degraders under anoxic conditions. Green anoxygenic bacteria
 534 participate on the carbon cycling and have been shown to fix CO₂ (Hug et al., 2013; Sirevåg,
 535 2004). The phototrophic communities of the microbial mats could be modified under A
 536 treatment leading to a higher relative abundance of green anoxygenic bacteria. It is also
 537 possible that the presence of more CO₂ on the environment conducted to a shift on the
 538 metabolism of green anoxygenic phototrophic bacteria fixing the CO₂ and being more
 539 competitive with the other communities.

540



541

542 **Figure 7:** Normalized absorption spectra of different pigments of the microbial mats. **A:**
 543 superimposed absorption spectra of the 6 detected chlorophyll derivatives (C deriv.). **B:**
 544 comparison between the absorption spectra of chlorophyll a (Ca) and C deriv. #2. **C:**

545 comparison between the absorption spectra of *Ca*, pheophytin *a* (Pha) and
546 bacteriochlorophyll *a* (BCa).

547

548 The bound carbohydrate EPS production was higher under the A treatment. EPS are
549 essential for maintaining the physical properties and proper functioning of microbial mats,
550 and are also involved in the adaptation of communities to their environment (Dupraz and
551 Visscher, 2005; Hubas, 2018; Prieto-Barajas et al., 2018). Therefore, EPS are an essential
552 element, even more when microorganisms are confronted with strong variations in physico-
553 chemical parameters. It has been observed that the degradation of polysaccharides by
554 bacterial extracellular enzymes is accelerated at low pH (Piontek et al., 2009). It can be
555 supposed that microbial mats could therefore synthesize more carbohydrates to compensate
556 for this degradation. Microbial mats in the W treatment did not show any variation in
557 concentration, suggesting that temperature has no effect on this process. Those in the WA
558 treatment also did not change suggesting that acidification and warming have probably
559 antagonistic effects limiting the impact of acidification on EPS. However, Li *et al.* (2016)
560 obtained contradictory results on three freshwater microalgae as they demonstrated that
561 acidification and warming act synergistically. The variation of bound carbohydrate EPS
562 suggest that microbial mats subjected to acidification modified their metabolism. Tan *et al.*
563 (2019) have shown that a polar strain of *Chlorella sp.* modulates its metabolism under
564 acidified conditions ($p\text{CO}_2 = 1000 \mu\text{atm}$), favouring its survival. They observed a decrease in
565 the fluxes of glucose and sucrose, the main products of photosynthesis, under high $p\text{CO}_2$.
566 Gong *et al.* (2020) also observed that the starch metabolism was modified by increasing the
567 quantity of starch granules in another microalgae named *Symbiochlorum hainanensis*. These
568 observations suggest that the organic carbon produced by photosynthesis in the microbial
569 mats placed under the A treatment was redirected towards the synthesis of other
570 carbohydrates which concentration had considerably increased.

571

572 **5. Conclusion**

573 The temperature in the warming treatments increased by 4°C from the initial temperature as
574 expected. Despite of a decrease of 0.4 unit pH in the water reserves of acidification
575 treatments, no significance difference was observed between the water pH of the different
576 treatments. The salinity increased on the warming treatments because of the water
577 evaporation. The dissolved oxygen concentration increased and was higher on the
578 acidification treatments, certainly due to an increase of the photosynthesis because of the
579 carbon input.

580 In the acidification treatment, our results showed that the concentration of bound
581 carbohydrates EPS increased. This indicated that the metabolisms were modified to cope
582 with the induced changes. In addition, the phototrophic communities of the microbial mats
583 under the different treatments showed characteristic pigments. In particular, unknown
584 chlorophyll derivatives were present under acidification and/or warming treatments. To the
585 best of our knowledge the synthesis of such derivatives following an acidification or/and a
586 warming experiment has never been reported before. These molecules were eventually
587 identified as bacteriochlorophyll *c* and several possible isomers which suggest that
588 experimentally induced climate change scenario may have favoured the increase of BC*c*
589 contained on green anoxygenic phototroph bacteria.

590 The mesocosm experiment has shown that phototrophic communities of the microbial mats
591 were able to adapt to the conditions defined by the IPCC (2014) regarding acidification and
592 warming of surface water. The most probable explanation is that the studied microbial mats
593 are already naturally confronted with environmental conditions (pH, light, temperature,
594 salinity, *etc.*) that fluctuate with a great amplitude in salt marshes. They may therefore
595 already be confronted with temperature and pH conditions predicted, for example, by the
596 IPCC for 2100. Changes in their metabolism probably enabled them to maintain a high
597 potential for photosynthetic activity when acidification took place. In the future, it would be
598 interesting to observe if a difference in the phylogenetic composition of these communities
599 occurred. This study provides new insights on the response of phototrophic communities of

600 microbial mats in a context of climatic change and permit to better understand their function
601 in this ecosystem.

602

603 **Acknowledgements**

604

605 C. Mazière was supported by a PhD grant from E2S-UPPA program and the Région
606 Nouvelle-Aquitaine. We thank the funding support from the European programme
607 ERANETMED AQUASALT (NMED-0003-01) and from the ACI politique d'établissement
608 Université de La Rochelle.

609 The authors are grateful to the salterns owner Michel Jauffrais and Thomas Lacoue-
610 Labarthe for his help in setting up the acidification treatment.

611

612 **References**

- 613 Aminot, A., Kérouel, R., 2007. Dosage automatique des nutriments dans les eaux marines., Quae. ed.
614 Baragi, L.V., Anil, A.C., 2016. Synergistic effect of elevated temperature, pCO₂ and nutrients on
615 marine biofilm. *Mar. Pollut. Bull.* 105, 102–109.
616 <https://doi.org/10.1016/j.marpolbul.2016.02.049>
617 Baragi, L.V., Khandeparker, L., Anil, A.C., 2015. Influence of elevated temperature and pCO₂ on the
618 marine periphytic diatom *Navicula distans* and its associated organisms in culture.
619 *Hydrobiologia* 762, 127–142. <https://doi.org/10.1007/s10750-015-2343-9>
620 Beardall, J., Stojkovic, S., Larsen, S., 2009. Living in a high CO₂ world: Impacts of global climate
621 change on marine phytoplankton. *Plant Ecol. Divers.* 2, 191–205.
622 <https://doi.org/10.1080/17550870903271363>
623 Black, J.G., Stark, J.S., Johnstone, G.J., McMinn, A., Boyd, P., McKinlay, J., Wotherspoon, S., Runcie,
624 J.W., 2019. In-situ behavioural and physiological responses of Antarctic microphytobenthos
625 to ocean acidification. *Sci. Rep.* 9, 1890. <https://doi.org/10.1038/s41598-018-36233-2>
626 Bolhuis, H., Stal, L.J., 2011. Analysis of bacterial and archaeal diversity in coastal microbial mats using
627 massive parallel 16S rRNA gene tag sequencing. *ISME J.* 5, 1701–1712.
628 <https://doi.org/10.1038/ismej.2011.52>
629 Bordenave, S., Fourçans, A., Blanchard, S., Goñi, M.S., Caumette, P., Duran, R., 2004a. Structure and
630 functional analyses of bacterial communities changes in microbial mats following petroleum
631 exposure. *Ophelia* 58, 195–203. <https://doi.org/10.1080/00785236.2004.10410227>
632 Bordenave, S., Goñi-urriza, M., Vilette, C., Blanchard, S., Caumette, P., Duran, R., 2008. Diversity of
633 ring-hydroxylating dioxygenases in pristine and oil contaminated microbial mats at genomic
634 and transcriptomic levels. *Environ. Microbiol.* 10, 3201–3211.
635 <https://doi.org/10.1111/j.1462-2920.2008.01707.x>
636 Bordenave, S., Jézéquel, R., Fourçans, A., Budzinski, H., Merlin, F.X., Fourel, T., Goñi-Urriza, M.,
637 Guyoneaud, R., Grimaud, R., Caumette, P., Duran, R., 2004b. Degradation of the “Erika” oil.
638 *Aquat. Living Resour.* 17, 261–267. <https://doi.org/10.1051/alr:2004027>

639 Brotas, V., Plante-Cuny, M.-R., 2003. The use of HPLC pigment analysis to study microphytobenthos
640 communities. *Acta Oecologica* 24. [https://doi.org/10.1016/S1146-609X\(03\)00013-4](https://doi.org/10.1016/S1146-609X(03)00013-4)
641 Cartaxana, P., Vieira, S., Ribeiro, L., Rocha, R., Cruz, S., Calado, R., Marques da Silva, J., 2015. Effects
642 of elevated temperature and CO₂ on intertidal microphytobenthos. *BMC Ecol.* 15, 10.
643 <https://doi.org/10.1186/s12898-015-0043-y>
644 Cavicchioli, R., Ripple, W.J., Timmis, K.N., Azam, F., Bakken, L.R., Baylis, M., Behrenfeld, M.J., Boetius,
645 A., Boyd, P.W., Classen, A.T., Crowther, T.W., Danovaro, R., Foreman, C.M., Huisman, J.,
646 Hutchins, D.A., Jansson, J.K., Karl, D.M., Koskella, B., Mark Welch, D.B., Martiny, J.B.H.,
647 Moran, M.A., Orphan, V.J., Reay, D.S., Remais, J.V., Rich, V.I., Singh, B.K., Stein, L.Y., Stewart,
648 F.J., Sullivan, M.B., van Oppen, M.J.H., Weaver, S.C., Webb, E.A., Webster, N.S., 2019.
649 Scientists' warning to humanity: microorganisms and climate change. *Nat. Rev. Microbiol.* 17,
650 569–586. <https://doi.org/10.1038/s41579-019-0222-5>
651 Cravo-Laureau, C., Duran, R., 2014. Marine coastal sediments microbial hydrocarbon degradation
652 processes: contribution of experimental ecology in the omics'era. *Front. Microbiol.* 5.
653 <https://doi.org/10.3389/fmicb.2014.00039>
654 Crawford, K.J., Raven, J.A., Wheeler, G.L., Baxter, E.J., Joint, I., 2011. The Response of *Thalassiosira*
655 *pseudonana* to Long-Term Exposure to Increased CO₂ and Decreased pH. *PLoS ONE* 6,
656 e26695. <https://doi.org/10.1371/journal.pone.0026695>
657 Decho, A., 2000. Microbial biofilms in intertidal systems: an overview. *Cont. Shelf Res.* 20, 1257–
658 1273. [https://doi.org/10.1016/S0278-4343\(00\)00022-4](https://doi.org/10.1016/S0278-4343(00)00022-4)
659 Decho, A., 1990. Decho AW.. Microbial exopolymer secretions in ocean environments: their role(s) in
660 food webs and marine processes. *Oceanogr Mar Biol Ann Rev* 28: 73-153. *Oceanogr. Mar.*
661 *Biol. Annu. Rev.* 28, 73–154.
662 Decho, A.W., Moriarty, D.J.W., 1990. Bacterial exopolymer utilization by a harpacticoid copepod: A
663 methodology and results. *Limnol. Oceanogr.* 35, 1039–1049.
664 <https://doi.org/10.4319/lo.1990.35.5.1039>
665 Dobretsov, S., Abed, R.M.M., Al Maskari, S.M.S., Al Sabahi, J.N., Victor, R., 2011. Cyanobacterial mats
666 from hot springs produce antimicrobial compounds and quorum-sensing inhibitors under
667 natural conditions. *J. Appl. Phycol.* 23, 983–993. <https://doi.org/10.1007/s10811-010-9627-2>
668 Dubois, Michel., Gilles, K.A., Hamilton, J.K., Rebers, P.A., Smith, Fred., 1956. Colorimetric Method for
669 Determination of Sugars and Related Substances. *Anal. Chem.* 28, 350–356.
670 <https://doi.org/10.1021/ac60111a017>
671 Dupraz, C., Visscher, P.T., 2005. Microbial lithification in marine stromatolites and hypersaline mats.
672 *Trends Microbiol.* 13, 429–438. <https://doi.org/10.1016/j.tim.2005.07.008>
673 Dutta, H., Dutta, A., 2016. The microbial aspect of climate change. *Energy Ecol. Environ.* 1, 209–232.
674 <https://doi.org/10.1007/s40974-016-0034-7>
675 Flemming, H.-C., Wingender, J., 2010. The biofilm matrix. *Nat. Rev. Microbiol.* 8, 623–633.
676 <https://doi.org/10.1038/nrmicro2415>
677 Fourçans, A., Oteyza, T.G. de, Wieland, A., Solé, A., Diestra, E., Bleijswijk, J. van, Grimalt, J.O., Kühl,
678 M., Esteve, I., Muyzer, G., Caumette, P., Duran, R., 2004. Characterization of functional
679 bacterial groups in a hypersaline microbial mat community (Salins-de-Giraud, Camargue,
680 France). *FEMS Microbiol. Ecol.* 51, 55–70. <https://doi.org/10.1016/j.femsec.2004.07.012>
681 Fourçans, A., Ranchou-Peyruse, A., Caumette, P., Duran, R., 2008. Molecular Analysis of the Spatio-
682 temporal Distribution of Sulfate-reducing Bacteria (SRB) in Camargue (France) Hypersaline
683 Microbial Mat. *Microb. Ecol.* 56, 90–100. <https://doi.org/10.1007/s00248-007-9327-x>
684 Fourçans, A., Solé, A., Diestra, E., Ranchou-Peyruse, A., Esteve, I., Caumette, P., Duran, R., 2006.
685 Vertical migration of phototrophic bacterial populations in a hypersaline microbial mat from
686 Salins-de-Giraud (Camargue, France). *FEMS Microbiol. Ecol.* 57, 367–377.
687 <https://doi.org/10.1111/j.1574-6941.2006.00124.x>
688 Frigaard, N.-U., Maqueo Chew, A.G., Maresca, J.A., Bryant, D.A., 2006. Bacteriochlorophyll
689 Biosynthesis in Green Bacteria, in: Grimm, B., Porra, R.J., Rüdiger, W., Scheer, H. (Eds.),

690 Chlorophylls and Bacteriochlorophylls, *Advances in Photosynthesis and Respiration*. Springer
691 Netherlands, Dordrecht, pp. 201–221. https://doi.org/10.1007/1-4020-4516-6_15

692 Gao, K., Helbling, E., Häder, D., Hutchins, D., 2012. Responses of marine primary producers to
693 interactions between ocean acidification, solar radiation, and warming. *Mar. Ecol. Prog. Ser.*
694 470, 167. <https://doi.org/10.3354/meps10043>

695 Gerola, A.P., Tsubone, T.M., Santana, A., de Oliveira, H.P.M., Hioka, N., Caetano, W., 2011. Properties
696 of Chlorophyll and Derivatives in Homogeneous and Microheterogeneous Systems. *J. Phys.*
697 *Chem. B* 115, 7364–7373. <https://doi.org/10.1021/jp201278b>

698 Gette-Bouvarot, M., Mermillod-Blondin, F., Lemoine, D., Delolme, C., Danjean, M., Etienne, L.,
699 Volatier, L., 2015. The potential control of benthic biofilm growth by macrophytes—A
700 mesocosm approach. *Ecol. Eng.* 75, 178–186. <https://doi.org/10.1016/j.ecoleng.2014.12.001>

701 Goedheer, J.C., 1966. Visible Absorption and Fluorescence of Chlorophyll and Its Aggregates in
702 Solution, in: *The Chlorophylls*. Elsevier, pp. 147–184. [https://doi.org/10.1016/B978-1-4832-](https://doi.org/10.1016/B978-1-4832-3289-8.50012-6)
703 [3289-8.50012-6](https://doi.org/10.1016/B978-1-4832-3289-8.50012-6)

704 Gong, S., Jin, X., Xiao, Y., Li, Z., 2020. Ocean Acidification and Warming Lead to Increased Growth and
705 Altered Chloroplast Morphology in the Thermo-Tolerant Alga *Symbiodinium hainanensis*.
706 *Front. Plant Sci.* 11. <https://doi.org/10.3389/fpls.2020.585202>

707 Hancke, K., Glud, R., 2004. Temperature effects on respiration and photosynthesis in three diatom-
708 dominated benthic communities. *Aquat. Microb. Ecol.* 37, 265–281.
709 <https://doi.org/10.3354/ame037265>

710 Hassenrück, C., Fink, A., Lichtschlag, A., Tegetmeyer, H.E., de Beer, D., Ramette, A., 2016.
711 Quantification of the effects of ocean acidification on sediment microbial communities in the
712 environment: the importance of ecosystem approaches. *FEMS Microbiol. Ecol.* 92.
713 <https://doi.org/10.1093/femsec/fiw027>

714 Hicks, N., Bulling, M.T., Solan, M., Raffaelli, D., White, P.C., Paterson, D.M., 2011. Impact of
715 biodiversity-climate futures on primary production and metabolism in a model benthic
716 estuarine system. *BMC Ecol.* 11, 7. <https://doi.org/10.1186/1472-6785-11-7>

717 Hiraishi, A., Shimada, K., 2001. Aerobic anoxygenic photosynthetic bacteria with zinc-
718 bacteriochlorophyll. *J. Gen. Appl. Microbiol.* 47, 161–180.
719 <https://doi.org/10.2323/jgam.47.161>

720 Hubas, C., 2018. Biofilms, tapis et agrégats microbiens : vers une vision unificatrice (HDR (Habilitation
721 à Diriger les Recherches)). Muséum National D’Histoire Naturelle.
722 <https://doi.org/10.5281/zenodo.3784703>

723 Hug, L.A., Castelle, C.J., Wrighton, K.C., Thomas, B.C., Sharon, I., Frischkorn, K.R., Williams, K.H.,
724 Tringe, S.G., Banfield, J.F., 2013. Community genomic analyses constrain the distribution of
725 metabolic traits across the Chloroflexi phylum and indicate roles in sediment carbon cycling.
726 *Microbiome* 1, 22. <https://doi.org/10.1186/2049-2618-1-22>

727 Hutchins, D.A., Fu, F., 2017. Microorganisms and ocean global change. *Nat. Microbiol.* 2, 17058.
728 <https://doi.org/10.1038/nmicrobiol.2017.58>

729 IPCC, 2014. *Climate Change 2014: Synthesis Report*. Contribution of Working Groups I, II and III
730 to the Fifth Assessment Report of the Intergovernmental Panel on Climate Change 169.

731 Jesus, B., Perkins, R.G., Mendes, C.R., Brotas, V., Paterson, D.M., 2006. Chlorophyll fluorescence as a
732 proxy for microphytobenthic biomass: alternatives to the current methodology. *Mar. Biol.*
733 150, 17–28. <https://doi.org/10.1007/s00227-006-0324-2>

734 Jorgensen, B.B., Revsbech, N.P., Cohen, Y., 1983. Photosynthesis and structure of benthic microbial
735 mats: Microelectrode and SEM studies of four cyanobacterial communities1. *Limnol.*
736 *Oceanogr.* 28, 1075–1093. <https://doi.org/10.4319/lo.1983.28.6.1075>

737 Kandler, N.M., Abdul Wahab, M.A., Noonan, S.H.C., Bell, J.J., Davy, S.K., Webster, N.S., Luter, H.M.,
738 2018. In situ responses of the sponge microbiome to ocean acidification. *FEMS Microbiol.*
739 *Ecol.* 94. <https://doi.org/10.1093/femsec/fiy205>

740 Li, W., Xu, X., Fujibayashi, M., Niu, Q., Tanaka, N., Nishimura, O., 2016. Response of microalgae to
741 elevated CO₂ and temperature: impact of climate change on freshwater ecosystems.
742 *Environ. Sci. Pollut. Res.* 23, 19847–19860. <https://doi.org/10.1007/s11356-016-7180-5>
743 Ma, J., Wang, P., Wang, X., Xu, Y., Paerl, H.W., 2019. Cyanobacteria in eutrophic waters benefit from
744 rising atmospheric CO₂ concentrations. *Sci. Total Environ.* 691, 1144–1154.
745 <https://doi.org/10.1016/j.scitotenv.2019.07.056>
746 Mackey, K., Morris, J., Morel, F., Kranz, S., 2015. Response of Photosynthesis to Ocean Acidification.
747 *Oceanography* 25, 74–91. <https://doi.org/10.5670/oceanog.2015.33>
748 Milenković, S.M., Zvezdanović, J.B., Anđelković, T.D., Marković, D.Z., 2012. THE IDENTIFICATION OF
749 CHLOROPHYLL AND ITS DERIVATIVES IN THE PIGMENT MIXTURES: HPLC-CHROMATOGRAPHY,
750 VISIBLE AND MASS SPECTROSCOPY STUDIES. *Adv. Technol.* 9.
751 Morrow, K.M., Bourne, D.G., Humphrey, C., Botté, E.S., Laffy, P., Zaneveld, J., Uthicke, S., Fabricius,
752 K.E., Webster, N.S., 2015. Natural volcanic CO₂ seeps reveal future trajectories for host-
753 microbial associations in corals and sponges. *ISME J.* 9, 894–908.
754 <https://doi.org/10.1038/ismej.2014.188>
755 Murata, N., Takahashi, S., Nishiyama, Y., Allakhverdiev, S.I., 2007. Photoinhibition of photosystem II
756 under environmental stress. *Biochim. Biophys. Acta BBA - Bioenerg., Structure and Function*
757 *of Photosystems* 1767, 414–421. <https://doi.org/10.1016/j.bbabi.2006.11.019>
758 Nagata, M., Yoshimura, Y., Inagaki, J., Suemori, Y., Iida, K., Ohtsuka, T., Nango, M., 2003. Construction
759 and Photocurrent of Light-harvesting Polypeptides/Zinc Bacteriochlorophyll *a* Complex in
760 Lipid Bilayers. *Chem. Lett.* 32, 852–853. <https://doi.org/10.1246/cl.2003.852>
761 Nishiyama, Y., Allakhverdiev, S.I., Murata, N., 2008. Regulation by Environmental Conditions of the
762 Repair of Photosystem II in Cyanobacteria, in: Demmig-Adams, B., Adams, W.W., Mattoo,
763 A.K. (Eds.), *Photoprotection, Photoinhibition, Gene Regulation, and Environment, Advances*
764 *in Photosynthesis and Respiration.* Springer Netherlands, Dordrecht, pp. 193–203.
765 https://doi.org/10.1007/1-4020-3579-9_13
766 Oelze, J., 1985. 9 Analysis of Bacteriochlorophylls**Dedicated to Prof. Dr. N. Pfennig on the occasion
767 of his 60th birthday in recognition of his numerous contributions on the ecology and
768 taxonomy of phototrophic bacteria., in: Bergan, T. (Ed.), *Methods in Microbiology.* Academic
769 Press, pp. 257–284. [https://doi.org/10.1016/S0580-9517\(08\)70478-1](https://doi.org/10.1016/S0580-9517(08)70478-1)
770 Peimbert, M., Alcaraz, L.D., Bonilla-Rosso, G., Olmedo-Alvarez, G., García-Oliva, F., Segovia, L.,
771 Eguiarte, L.E., Souza, V., 2012. Comparative Metagenomics of Two Microbial Mats at Cuatro
772 Ciénegas Basin I: Ancient Lessons on How to Cope with an Environment Under Severe
773 Nutrient Stress. *Astrobiology* 12, 648–658. <https://doi.org/10.1089/ast.2011.0694>
774 Pierson, B.K., Castenholz, R.W., 1974. A phototrophic gliding filamentous bacterium of hot springs,
775 *Chloroflexus aurantiacus*, gen. and sp. nov. *Arch. Microbiol.* 100, 5–24.
776 <https://doi.org/10.1007/BF00446302>
777 Piontek, J., Lunau, M., Händel, N., Borchard, C., Wurst, M., Engel, A., 2009. Acidification increases
778 microbial polysaccharide degradation in the ocean. *Biogeosciences Discuss.* 7.
779 <https://doi.org/10.5194/bg-7-1615-2010>
780 Prieto-Barajas, C.M., Valencia-Cantero, E., Santoyo, G., 2018. Microbial mat ecosystems: Structure
781 types, functional diversity, and biotechnological application. *Electron. J. Biotechnol.* 31, 48–
782 56. <https://doi.org/10.1016/j.ejbt.2017.11.001>
783 Rae, B.D., Long, B.M., Badger, M.R., Price, G.D., 2013. Functions, Compositions, and Evolution of the
784 Two Types of Carboxysomes: Polyhedral Microcompartments That Facilitate CO₂ Fixation in
785 Cyanobacteria and Some Proteobacteria. *Microbiol. Mol. Biol. Rev. MMBR* 77, 357–379.
786 <https://doi.org/10.1128/MMBR.00061-12>
787 Redfield, A.C., 1958. The biological control of chemical factors in the environment. *Am. Sci.* 46, 230A–
788 221.
789 Reinold, Wong, MacLeod, Meltzer, Thompson, Burns, 2019. The Vulnerability of Microbial
790 Ecosystems in A Changing Climate: Potential Impact in Shark Bay. *Life* 9, 71.
791 <https://doi.org/10.3390/life9030071>

792 Revsbech, N.P., Jorgensen, B.B., Blackburn, T.H., Cohen, Y., 1983. Microelectrode studies of the
793 photosynthesis and O₂, H₂S, and pH profiles of a microbial mat¹. *Limnol. Oceanogr.* 28,
794 1062–1074. <https://doi.org/10.4319/lo.1983.28.6.1062>

795 Scheer, H., 2006. An Overview of Chlorophylls and Bacteriochlorophylls: Biochemistry, Biophysics,
796 Functions and Applications, in: Grimm, B., Porra, R.J., Rüdiger, W., Scheer, H. (Eds.),
797 Chlorophylls and Bacteriochlorophylls: Biochemistry, Biophysics, Functions and Applications,
798 Advances in Photosynthesis and Respiration. Springer Netherlands, Dordrecht, pp. 1–26.
799 https://doi.org/10.1007/1-4020-4516-6_1

800 Sirevåg, R., 2004. Carbon Metabolism in Green Bacteria, in: Blankenship, R.E., Madigan, M.T., Bauer,
801 C.E. (Eds.), Anoxygenic Photosynthetic Bacteria, Advances in Photosynthesis and Respiration.
802 Kluwer Academic Publishers, Dordrecht, pp. 871–883. [https://doi.org/10.1007/0-306-47954-](https://doi.org/10.1007/0-306-47954-0_40)
803 [0_40](https://doi.org/10.1007/0-306-47954-0_40)

804 Sørensen, K.B., Canfield, D.E., Teske, A.P., Oren, A., 2005. Community Composition of a Hypersaline
805 Endoevaporitic Microbial Mat. *Appl. Environ. Microbiol.* 71, 7352–7365.
806 <https://doi.org/10.1128/AEM.71.11.7352-7365.2005>

807 Stauffert, M., Cravo-Laureau, C., Jezequel, R., Barantal, S., Cuny, P., Gilbert, F., Cagnon, C., Milton, C.,
808 Amouroux, D., Mahdaoui, F., Bouyssièrè, B., Stora, G., Merlin, F., Duran, R., 2013. Impact of
809 Oil on Bacterial Community Structure in Bioturbated Sediments. *PloS One* 8, e65347.
810 <https://doi.org/10.1371/journal.pone.0065347>

811 Takahashi, E., Ledauphin, J., Goux, D., Orvain, F., 2009. Optimising extraction of extracellular
812 polymeric substances (EPS) from benthic diatoms: Comparison of the efficiency of six EPS
813 extraction methods. *Mar. Freshw. Res.* 60, 1201–1210. <http://dx.doi.org/10.1071/MF08258>

814 Tan, Y.-H., Lim, P.-E., Beardall, J., Poong, S.-W., Phang, S.-M., 2019. A metabolomic approach to
815 investigate effects of ocean acidification on a polar microalga *Chlorella* sp. *Aquat. Toxicol.*
816 217, 105349. <https://doi.org/10.1016/j.aquatox.2019.105349>

817 Underwood, G.J.C., Boulcott, M., Raines, C.A., Waldron, K., 2004. Environmental Effects on
818 Exopolymer Production by Marine Benthic Diatoms: Dynamics, Changes in Composition, and
819 Pathways of Production¹. *J. Phycol.* 40, 293–304. [https://doi.org/10.1111/j.1529-](https://doi.org/10.1111/j.1529-8817.2004.03076.x)
820 [8817.2004.03076.x](https://doi.org/10.1111/j.1529-8817.2004.03076.x)

821 Uribe-Lorío, L., Brenes-Guillén, L., Hernández-Ascencio, W., Mora-Amador, R., González, G., Ramírez-
822 Umaña, C.J., Díez, B., Pedrós-Alió, C., 2019. The influence of temperature and pH on bacterial
823 community composition of microbial mats in hot springs from Costa Rica. *MicrobiologyOpen*
824 8. <https://doi.org/10.1002/mbo3.893>

825 van Gemerden, H., 1993. Microbial mats: A joint venture. *Mar. Geol.* 113, 3–25.
826 [https://doi.org/10.1016/0025-3227\(93\)90146-M](https://doi.org/10.1016/0025-3227(93)90146-M)

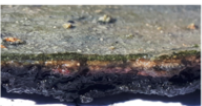
827 Wang, S., Zhang, D., Pan, X., 2013. Effects of cadmium on the activities of photosystems of *Chlorella*
828 *pyrenoidosa* and the protective role of cyclic electron flow. *Chemosphere* 93, 230–237.
829 <https://doi.org/10.1016/j.chemosphere.2013.04.070>

830 Wang, X., Feng, X., Zhuang, Y., Lu, J., Wang, Y., Gonçalves, R.J., Li, X., Lou, Y., Guan, W., 2019. Effects
831 of ocean acidification and solar ultraviolet radiation on physiology and toxicity of
832 dinoflagellate *Karenia mikimotoi*. *Harmful Algae* 81, 1–9.
833 <https://doi.org/10.1016/j.hal.2018.11.013>

834 Wieland, A., Köhl, M., McGowan, L., Fourçans, A., Duran, R., Caumette, P., Garcia de Oteyza, T.,
835 Grimalt, J.O., Solé, A., Diestra, E., Esteve, I., Herbert, R.A., 2003. Microbial Mats on the
836 Orkney Islands Revisited: Microenvironment and Microbial Community Composition. *Microb.*
837 *Ecol.* 46, 371–390. <https://doi.org/10.1007/s00248-002-0108-2>

838 Wootton, J.T., Pfister, C.A., Forester, J.D., 2008. Dynamic patterns and ecological impacts of declining
839 ocean pH in a high-resolution multi-year dataset. *Proc. Natl. Acad. Sci.* 105, 18848–18853.
840 <https://doi.org/10.1073/pnas.0810079105>

841 Yue, F., Gao, G., Ma, J., Wu, H., Li, X., Xu, J., 2019. Future CO₂-induced seawater acidification
842 mediates the physiological performance of a green alga *Ulva linza* in different photoperiods.
843 *PeerJ* 7. <https://doi.org/10.7717/peerj.7048>



Control
20°C – pH = 8

Acidification treatment
20°C – pH =
7.6

Warming treatment
24°C – pH = 8

**Acidification +
warming treatment**
24°C – pH =
7.6

Photosynthetic efficiency	=	=	=	=
Extracellular polymeric substances	=	+ (bound carbohydrates EPS)	=	=
Chlorophyll a	=	-	=	=
Chlorophyll derivatives	=	+	=	=



Change in the phototrophic communities

OR

Change in the metabolism of green anoxygenic phototroph bacteria